CHEMISTRY OF MATERIALS

ARTICLE

pubs.acs.org/cm

Structural Complexity and Electrical Properties of the Garnet-Type Structure $LaLi_{0.5}Fe_{0.2}O_{2.09}$ Studied by ^{7}Li and ^{139}La Solid State NMR Spectroscopy and Impedance Spectroscopy

T.L. Spencer,[†] Adam Ramzy,[‡] V. Thangadurai,*[,‡] and G. R. Goward*[,†]

[†]Department of Chemistry and Brockhouse Institute for Materials Research, McMaster University, 1280 Main Street, W. Hamilton, Ontario L8S 4M1, Canada

[‡]Department of Chemistry, University of Calgary, 2500 University Drive NW, Calgary, Alberta T2N 1N4, Canada

ABSTRACT: Garnet-like structures containing lithium are of interest for applications in lithium ion batteries because of their inherent lithium ion conductivity and stability against chemical reaction with Li. Here, a series of materials, with parent composition $LaLi_{0.5}Fe_{0.2}O_{2.09}$, are synthesized using solid-state chemistry, and characterized, in terms of their structure, using a combination of powder X-ray diffraction (PXRD), ^{7}Li, and ^{139}La solid-state NMR, which reveal disorder on the Li and Fe sites in the lattice. The ^{7}Li spectra comprise a set of peaks that are distinguished based on their T_1 relaxation properties, as a diamagnetic set and a paramagnetic set of peaks. The ^{139}La spectra include two La environments, one well-defined, with a C_Q of 56 MHz ± 1 MHz and asymmetry parameter, η of 0.05 ± 0.05, and a second, which experiences a range of local environments, because of the Li/Fe substitution, and has a C_Q of 29 MHz ± 2 MHz, and η of 0.6 ± 0.1. The dynamics within the materials were characterized using impedance spectroscopy, and trends were correlated with the lithium content and structural features. The best conductivity was determined for the parent material, $LaLi_{0.5}Fe_{0.2}O_{2.09}$, after sintering at 850 °C. The complex ^{7}Li and ^{139}La NMR spectra, interpreted together with (PXRD) data, indicate that the increasing concentration of lithium in the material populates an iron site with excess lithium, in a range of possible local environments, which appears to decrease the total ionic and electronic conductivity.

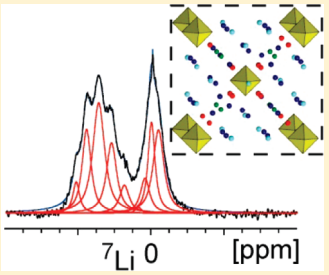

KEYWORDS: solid-state electrolytes, lithium ion conductors, solid-state NMR, ^{139}La NMR, ^{7}Li NMR, lithium ion batteries, ac impedance spectroscopy

INTRODUCTION

Garnet-like structures containing heavy elements have attracted great interest because of their intriguing structures and properties.[1−3] Synthetic garnet structures have attracted interest in many different fields of chemistry, including crystallography, where the determination of site occupancies of specific ions in the compound is of interest.[4] Garnet structures also exhibit interesting properties such as luminescence in bismuth-containing structures.[5] In recent years lithium-containing garnet structures have been recognized as potential electrolytes for use in Li ion batteries.[1−3] Several garnet structures are known to conduct Li ions, while being electrical resistors, allowing them to have potential applications as electrolyte materials in Li ion batteries. Others are known to conduct electrons, creating the possibility for use as electrode materials in Li ion batteries, provided that an appropriate redox couple is present.[1]

The mechanism of conductivity in the lithium-containing garnet structures has been studied by several groups.[2,3,6−8] Ramzy and Thangadurai have shown a simple empirical relation between concentration of Li and ionic conductivity in the several garnet-type compounds.[9] The ionic conductivity seems to increases with increase in Li in the iso structure (cubic) garnet-type compounds, for example, $Li_5La_3Ta_2O_{12}$, $Li_6La_2BaTa_2O_{12}$, and $Li_7La_3Zr_2O_{12}$.[8] More importantly, the occupation of Li ion in various crystallographic sites directly controls the ionic conductivity in the garnet-type structures.[10] The most commonly proposed mechanism is that of a jumping motion of Li between face sharing octahedral sites.[11] The Li ions disperse among the different sites to prevent excessively short Li−Li distances caused by neighboring tetrahedral and octahedral sites that are face sharing and create Li−Li distances of <2.4 Å.[12] O'Callaghan and Cussen performed an in-depth neutron diffraction study on Li excess in $Li_{5+x}Ba_xLa_{3-x}Ta_2O_{12}$ ($0 < x \leq 1.6$) garnets to understand Li ion occupation and its relationship to the conductivity.[10] In the cubic garnet-type structure, the tetrahedral site acts as essentially a Li ion trap, but the other octahedral sites typically have high mobility and facilitate high ionic conductivity.[3]

$^{6,7}Li$ solid-state magic angle spinning (MAS) nuclear magnetic resonance (NMR) is a useful tool to study structure and dynamics in potential Li ion battery materials.[6,7] In particular, it is important to distinguish between Li ions in tetrahedral and octahedral environments, to describe site-specific ionic conductivity mechanisms. This has been elucidated recently in a $^{6,7}Li$ MAS NMR study of the electrolyte material, $Li_5La_3Nb_2O_{12}$, where it was determined that Li ion conduction occurs in the octahedral sites.[3] Solid-state $^{6,7}Li$ NMR served as a useful tool to determine the relative octahedral to tetrahedral site occupancies

Received: March 22, 2011
Revised: May 6, 2011
Published: June 02, 2011

of materials made with different ratios of tetrahedral and octahedral Li sites. This allowed a correlation to be made between the amount of Li in the octahedral site and the measured Li ion conductivity of the materials.[3]

^{6}Li MAS NMR has an advantage over ^{7}Li MAS NMR, because of its smaller magnetogyric ratio and smaller quadrupole moment, both of which lead to narrower lines.[13] The disadvantage, however, to measuring ^{6}Li in diamagnetic samples is the long T_1 relaxation times, which can exceed several minutes. This is in addition to its low natural abundance.[3,13] The challenge of long relaxation times may be overcome by studying paramagnetic materials, which contain unpaired electrons which shorten the relaxation time of the lithium nuclei. Paramagnetic materials often exhibit spectral peaks over a much wider range of chemical shifts than their diamagnetic counterparts.[14,15]

As well as the lithium nuclei, the lanthanum nuclei can also provide important structural information in the garnet materials of interest. We show here that ^{139}La NMR can be use to distinguish between La crystallographic sites, and when combined with ^{7}Li MAS NMR can give insight into the crystal structure of the material. ^{139}La has a spin of 7/2 and produces wide spectra with large values of quadrupolar coupling, C_Q; thus, the excitation of the full central transition is difficult using traditional solid-state echo experiments.[16] The WURST-QCPMG and WURST-echo experiments prove to be very useful to study the full ^{139}La spectra of battery materials.[17−19] With these NMR pulse sequences, there is an advantage of a wide, 1 MHz, excitation profile because of the swept frequency "adiabatic" pulse that is provided by a WURST pulse shape.[17] The effect of the pulse sequences that employ a WURST pulse shape is greatly enhanced at higher magnetic field, where the increased field strength narrows the spectral lines, and allows the full spectra of the materials of interest to be collected in only one NMR experiment. This is an improvement over traditional methods of frequency stepped NMR experiments, in which the excitation frequency is moved sequentially over several experiments to excite the full width of the central transition.[20−22]

In this study, for the first time, we report the synthesis, structure, electrical transport properties of Fe-based garnet-related structures $LaLi_{0.5}Fe_{0.2}O_{2.09}$, $La_{0.94}Li_{0.69}Fe_{0.2}O_{2.09}$, and $LaLi_{0.75}Fe_{0.14}O_{2.09}$ together with ^{7}Li and ^{139}La solid-state NMR characterization. The parent garnet-like $LaLi_{0.5}Fe_{0.2}O_{2.09}$ was first prepared by Mazza and coworkers in 1985.[23−25] It has been shown to conduct lithium ions as well as electrons, and has a redox couple between Fe^{3+} and Fe^{4+}. It is therefore a potential material for use as a cathode in Li ion batteries.[24] Although this material has not been cycled electrochemically, it can be expected that there will be a high voltage plateau, such as that found for the Fe^{3+}/Fe^{4+} couple in $Li[Fe_yMn_{2-y}]O_4$ at ∼5 V.[26] As such, it would be viable in the context of all-solid-state Li ion cells, with the possibility of incorporating a complementary garnet structured solid-state electrolyte.[27]

The theoretical fully occupied parent compound for this series of structures is $La_{1.1}Li_{0.5}Fe_{0.31}O_{2.5}$.[24] It has been determined that this compound does not exist in this fully occupied state, but rather has a series of vacancies present. These are distributed over the compound and are found in varying amounts on each atomic position, except that of Li.[24] In particular, the vacancies reported on the Fe sites at (0, 0, 0) and (0.25, 0.25, 0.25) are significant, as will be discussed further in this work. This structure opens the possibility of Li ion dynamics, via vacancy-mediated conductivity. Moreover, our studies provide evidence, for the first time, of Li−Fe substitution in these garnet structures. Precedent for this is seen in the $LiFePO_4$ phase, where such anti-site defects have been shown to create channel-blocking iron centers in this one-dimensional (1D) Li ion conductor.[28]

In this work the effect of synthesis temperature conditions and stoichiometry is examined in relation to total ionic and electronic conductivity of garnet-like materials derived from $LaLi_{0.5}Fe_{0.2}O_{2.09}$.[24] ^{7}Li and ^{139}La solid-state NMR are used for structural determination, while impedance measurements are used to determine the electrical transport properties.

EXPERIMENTAL SECTION

Synthesis and Electrical Characterization. Compounds of the nominal chemical formula of $LaLi_{0.5}Fe_{0.2}O_{2.09}$, $La_{0.94}Li_{0.69}Fe_{0.2}O_{2.09}$, and $LaLi_{0.75}Fe_{0.14}O_{2.09}$ were prepared via a conventional solid-state reaction (ceramic method) using stoichiometric quantities of high purity $LiNO_3$ (GR, 97%, EM Science), La_2O_3 (99.99%, Alfa Aesar), and Fe_2O_3 (99+ %, Alfa Aesar). The reactants were weighed and ball-milled employing a Pulverisette, Fritsch, Germany, ball mill at 200 rpm for 3 h with zirconium balls in 2-propanol. As reported in the garnet-type materials synthesis, 10 wt % excess $LiNO_3$ was added to account for loss of Li oxide during sintering. A similar synthesis method has been used to prepare garnet-type materials in the literature.[4,5,8] After mixing and drying at room temperature, samples were heated at 600 °C to decompose the metal salts. Samples were then reground for 6 h and powder samples were pressed into pellets under isostatic pressure. Pellets were then sintered at 800 and 850 °C for 16−20 h. Powder X-ray diffraction (PXRD; Bruker D8 powder X-ray diffractometer (Cu Kα, 40 kV, 40 mA)) was employed for phase formation characterization. After confirmation of successful a single-phase structure, pellets were painted with Au electrodes (paste, cured at 600 °C for 1 h) for electrical conductivity employing a Solarton SI 1260 impedance and gain-phase analyzer in the frequency range of 0.1 to 10×10^6 Hz in air.

^{7}Li MAS and ^{139}La Static NMR Spectroscopy. ^{7}Li MAS NMR was collected at 11.7 T (Larmor frequency, 194.4 MHz) on a Bruker Avance I 500 NMR spectrometer with an external reference of 1 M LiCl solution, at 0 ppm, having a 90° pulse length of 4 μs at 1.25 dB. A 2.5 mm probe was used, with a rotor spinning speed of 20 kHz, and solid-state ^{7}Li MAS spectra were collected using a 1 μs ($\pi/8$) pulse, with a relaxation delay of 20 s. T_1 relaxation measurements were performed at 21.1 T for ^{7}Li in $La_{0.94}Li_{0.69}Fe_{0.2}O_{2.09}$. An inversion recovery pulse sequence was used, with a variable delay list of 16 values. A recycle delay of 30 s was used in the first experiment; and a recycle delay of 450 s was used in the second experiment. The experiment was performed twice to account for the great differences in T_1 relaxation properties of the lithium sites in the material. In each measurement 32 transients were collected; a pulse length of 4.5 μs was used with a power level of 6.00 dB.

Because of the difference in spin−lattice relaxation times (T_1) of the paramagnetic and diamagnetic lithium peaks, in particular the very long T_1 of the diamagnetic peak at 0 ppm, it was necessary to use a fractional pulse of $\pi/8$ to allow the diamagnetic peaks to fully relax with a 20 s recycle delay. A much longer time is necessary for the full relaxation of the diamagnetic peak if a 90° pulse is used.

^{139}La solid-state static NMR was performed at 21.1 T using a Bruker Avance II 900 NMR spectrometer at the National Ultrahigh-Field NMR Facility for Solids (http://www.nmr900.ca). An external reference was used, a 1 M solution of $LaCl_3$ (0 ppm), for which a 180° pulse had a pulse length of 16.0 μs at 3.30 dB. Typically in the WURST-QCPMG experiments 50 μs WURST pulses were applied with a range of 1 MHz and a rate of 20 MHz/ms. An RF power of 10 kHz was used, and the spikelet-separation was 2.5 kHz. The number of echoes in a QCPMG train ranged from 32 to 64. Recycle delays of 0.2−0.5 s were found sufficient for complete relaxation.

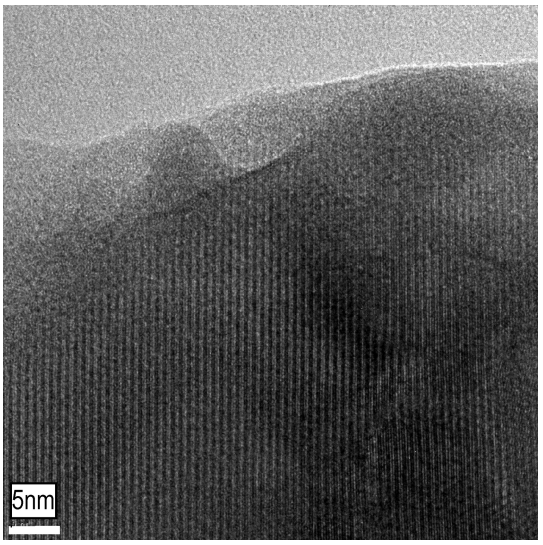

Figure 1. Typical TEM image of $LaLi_{0.5}Fe_{0.2}O_{2.09}$. The image was taken on an FEI Titan 80-300 equipped with an image aberration corrector operated at 300 kV. TEM analysis showed a single phase, with a high degree of crystallinity.

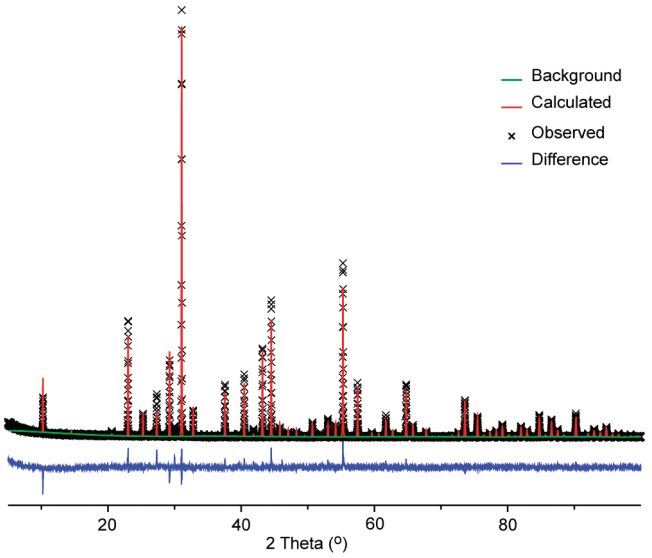

Figure 2. GSAS Rietveld refinement output for $LaLi_{0.5}Fe_{0.2}O_{2.09}$. Parameters used for the refinement were taken from the literature.[24] χ^2 was found to be 2.5.

RESULTS AND DISCUSSION

Structural Analysis. PXRD shows the formation of single-phase garnet-type structure for $LaLi_{0.5}Fe_{0.2}O_{2.09}$, $La_{0.94}Li_{0.69}Fe_{0.2}O_{2.09}$, and $LaLi_{0.75}Fe_{0.14}O_{2.09}$ and the observed line match with parent compound $LaLi_{0.5}Fe_{0.2}O_{2.09}$, as reported by Mazza and coworkers in 1985.[23−25] A transmission electron microscopy (TEM) image of $LaLi_{0.5}Fe_{0.2}O_{2.09}$ indicates a highly crystalline structure, with *d*-spacing of 0.40 nm, and is shown in Figure 1. Similar TEM analysis was performed for the other investigated materials.

Rietveld refinement on the PXRD pattern using GSAS was also performed and is shown in Figure 2 for $LaLi_{0.5}Fe_{0.2}O_{2.09}$.[29]

Table 1. Rietveld Refinement Structural Parameters for $LaLi_{0.5}Fe_{0.2}O_{2.09}$[a]

atom	*x*	*y*	*z*	multiplicity	occupancy
La-1	0.00000	0.30431(8)	0.30431(8)	24	1.0000
La-2	0.34548(8)	0.00000	0.00000	12	1.0000
Fe-1	0.00000	0.00000	0.00000	2	1.0000
Fe-2	0.25000	0.25000	0.25000	8	0.9305
O-1	0.36471(1)	0.36471(1)	0.20633(5)	48	1.0000
O-2	0.25000	0.50000	0.00000	12	1.0000
O-3	0.13908(1)	0.50000	0.00000	24	1.0000
O-4	0.00000	0.13059(1)	0.00000	12	1.0000
Li	0.15894(4)	0.15894(4)	0.15894(4)	16	1.0000

[a] Note: For the $LaLi_{0.5}Fe_{0.2}O_{2.09}$ in space group $Im\bar{3}m$, $a = b = c = 12.2032 \pm 0.0002$ Å; $\alpha = \beta = \gamma = 90°$; $\chi^2 = 2.5$.

There is a small peak in the PXRD at 30°, which is due to a small Li_2O impurity.[30] Table 1 lists the Rietveld refinement structure parameters of $LaLi_{0.5}Fe_{0.2}O_{2.09}$ for comparison and is consistent with literature.[13−15] PXRD is known to be insensitive to Li; therefore, it can be expected that ^{7}Li NMR would give a more accurate measurement of the Li environments in this sample.

^{7}Li and ^{139}La NMR of La−Li−Fe Oxide Series. Previous structural characterization of $LaLi_{0.5}Fe_{0.2}O_{2.09}$ using PXRD found a cubic structure in space group $Im\bar{3}m$, with a single crystallographically unique Li site at (0.133, 0.133, 0.133).[24] Noting that Li is difficult to locate by X-ray methods, because of its low scattering factor, it was nevertheless anticipated that the ^{7}Li NMR spectrum of the material would consist of a single resonance, possibly shifted to higher frequency because of the paramagnetic influence of the iron centers. In contrast, a standard ^{7}Li MAS NMR examination of this material, using ^{7}Li MAS NMR at 11.7 T revealed multiple Li sites, as shown in Figure 3.

From the ^{7}Li MAS NMR taken at 11.7 T, it is evident that the Li exists in a distribution of sites, ranging in chemical shift from ∼20 ppm to ∼ −1 ppm, shown in Table 2. The possibility of this array of Li sights being caused by the effect of Li coupling to La was ruled out when the Li spectrum of this material was studied at a higher magnetic field, 21.1 T. The spacing of the peaks is equal in units of parts per million (ppm) at both fields, while the spacing in hertz (Hz) is different. This is consistent with NMR peaks that are separated because of chemical shift alone,[31] thereby indicating several unique local environments of the lithium ions. In addition to a complex NMR spectrum, this compound shows interesting ^{7}Li T_1 relaxation properties via the ^{7}Li MAS NMR: the ^{7}Li NMR peaks represent two groups of Li environments with different magnetic properties: paramagnetic and diamagnetic as indicated by the large difference in values of T_1 for different peaks that were observed in NMR spectra. T_1 measurements of $La_{0.94}Li_{0.69}Fe_{0.2}O_{2.09}$ were analyzed separately in two regions. The site at 14.5 ppm has a short T_1, 11.45 ± 0.06 ms, suggesting that it is paramagnetic in nature. This may be due to its proximity to an Fe atom in the compound, since Fe contains unpaired electrons and will contribute to the paramagnetic nature of nearby Li sites.[15] The Li site at ∼0 ppm has a very long T_1, > 10.9×10^4 ms, suggesting that it is diamagnetic, and comparatively far from Fe atoms, and unpaired electrons, in this compound.

Figure 4 shows the chemical shift trends for each of the lithium peaks in the ^{7}Li MAS NMR spectrum of $La_{0.94}Li_{0.69}Fe_{0.2}O_{2.09}$, as a function of temperature. The steeper slope of the data with

dx.doi.org/10.1021/cm200823p |*Chem. Mater.* 2011, 23, 3105–3113

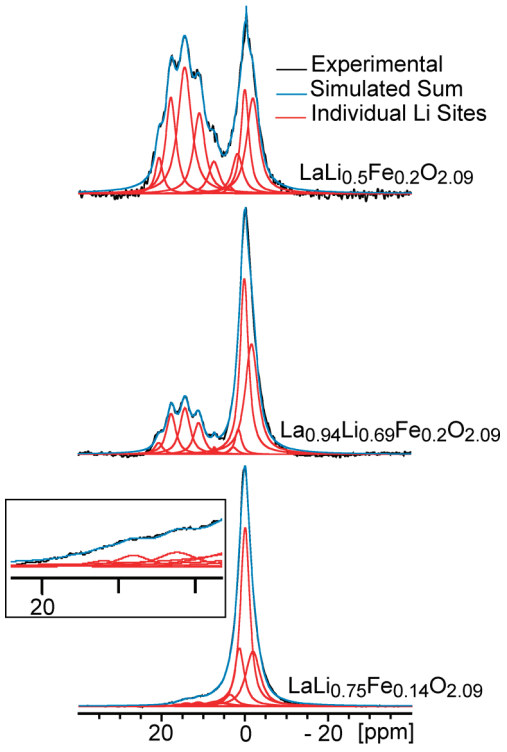

Figure 3. ^{7}Li MAS NMR of $LaLi_{0.5}Fe_{0.2}O_{2.09}$ (top) collected at 11.7 T, with a spinning speed of 20 kHz. This shows multiple peaks that represent different Li sites in the sample, with line fit analysis performed in the TopSpin 2.1 software. The experimental spectrum is shown in black, while the simulated sites are shown in red, and their sum is shown in blue. The ^{7}Li MAS NMR of $La_{0.94}Li_{0.69}Fe_{0.2}O_{2.09}$ and $LaLi_{0.75}Fe_{0.14}O_{2.09}$ are shown when measured under the same conditions as $LaLi_{0.5}Fe_{0.2}O_{2.09}$. Line fit analysis was performed with the same number of peaks contributing to the spectrum. The full peak analysis is shown in Table 2.

higher chemical shifts is consistent with the expected Curie–Weiss behavior of the peaks experiencing paramagnetic interactions, arising from the temperature dependence of the magnetic susceptibility.[32] This supports the differences observed in the T_1 values obtained by NMR for ^{7}Li, with the lowest T_1 observed for peaks that result in a larger slope in the plot of chemical shift versus inverse temperature. On the basis of the unexpected number of ^{7}Li NMR resonances observed, we evaluated the structure in more detail, and in particular, the possibility of substitution of Li onto the Fe lattice sites is determined to justify the range of chemical shifts observed.

Different combinations of the positions of Li and Fe were attempted in the refinement, and it was found that there is a potential for Li to partially occupy the Fe site at (0.25, 0.25, 0.25); whereas occupancy of the (0, 0, 0) Fe site by Li was not found as a solution by the software, suggesting that there only Li substitution on the (0.25, 0.25, 0.25) Fe site. Figure 5 shows an image of the unit cell of $LaLi_{0.5}Fe_{0.2}O_{2.09}$ for a situation in which there is a total substitution of iron for Li on the (0.25, 0.25, 0.25) site. This is the extreme case, and it is more likely that a partial replacement of Fe by Li occurs on this site. This rearrangement only accounts for one additional Li site, while the NMR predicts several different sites.

This structure is known to have vacancies, some of which exist on the iron (0.25, 0.25, 0.25) site (green spheres in Figure 5).[24]

Table 2. Line Width Analysis of ^{7}Li MAS NMR of $LaLi_{0.5}Fe_{0.2}O_{2.09}$, $La_{0.94}Li_{0.69}Fe_{0.2}O_{2.09}$, and $LaLi_{0.75}Fe_{0.14}O_{2.09}$

	$LaLi_{0.5}Fe_{0.2}O_{2.09}$								
peak shift (in ppm ± 0.5 ppm)	20.7	17.9	14.5	11	7.5	3.7	1.8	0.1	−1.9
line width (in Hz ± 20 Hz)	420	570	750	650	610	370	590	450	690
% contribution (± 1%)	25	14	15	5	4	1	17	12	6
	$La_{0.94}Li_{0.69}Fe_{0.2}O_{2.09}$								
peak shift (in ppm ± 0.5 ppm)	20.6	17.6	14.3	11.1	7.3	2.7	1.5	0.1	−1.7
line width (Hz)	440	520	570	540	190	430	370	470	710
% contribution (± 1%)	11	7	9	1	2	1	32	34	4
	$LaLi_{0.75}Fe_{0.14}O_{2.09}$								
peak shift (in ppm ± 0.5 ppm)	18.2	16	14.2	11.4	7.1	3.7	1.5	0.1	−1.8
line width (Hz) ± 20 Hz	290	510	450	570	1070	630	550	520	800
% contribution (± 1%)	0.8	1.0	0.4	3	0.1	4	24	50	17

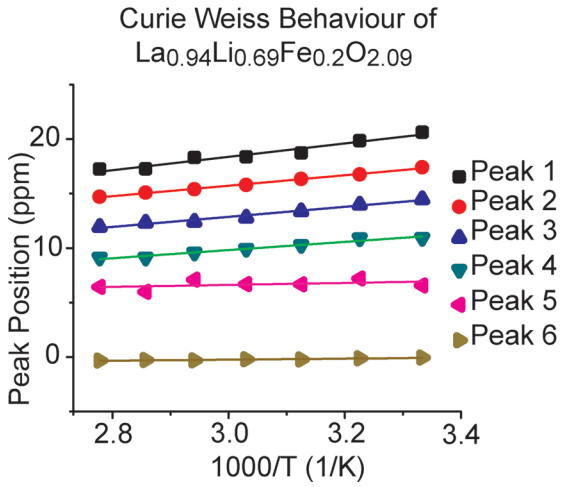

Figure 4. Curie–Weiss behavior of peaks in ^{7}Li NMR spectrum of $La_{0.94}Li_{0.69}Fe_{0.2}O_{2.09}$. Peaks are numbers from highest frequency to lowest frequency. Peak 6 represents the center of gravity of the diamagnetic peaks at ~0 ppm.

A vacancy may also exist on the Li site, since it is possible for the Li to move onto a vacant Fe site, and thus be replaced by the vacancy. This introduces the possibility of a distribution of Li sites, in which different Li environments are created by having different proximities to Fe, and therefore the unpaired electrons in the system. Li atoms that are close to Fe in the crystal structure are expected to have a larger paramagnetic nature, and thus a higher chemical shift and shorter T_1 relaxation time, than those that are farther from Fe. As a result of the Li being spread over a distribution of sites, the site at (0.25, 0.25, 0.25) can be seen as a variable site itself, given that it can be occupied by either Li, Fe, or a vacant site.

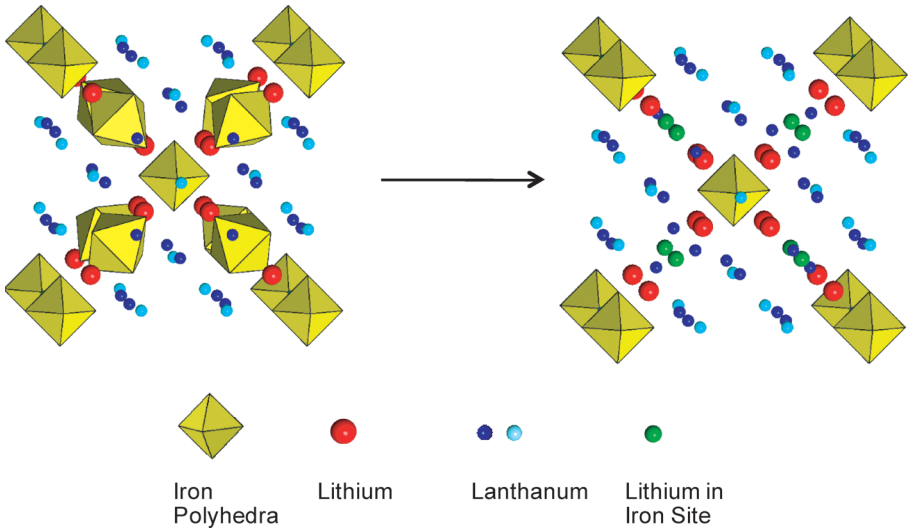

Figure 5. Right: XtalDraw image of $LaLi_{0.5}Fe_{0.2}O_{2.09}$.[33] This is a cubic structure in space group $Im\bar{3}m$, with cell length 12.231 Å. Left: XtalDraw image of structure in which all of the Fe (0.25, 0.25, 0.25) sites have been replaced by Li, shown as the green ions.

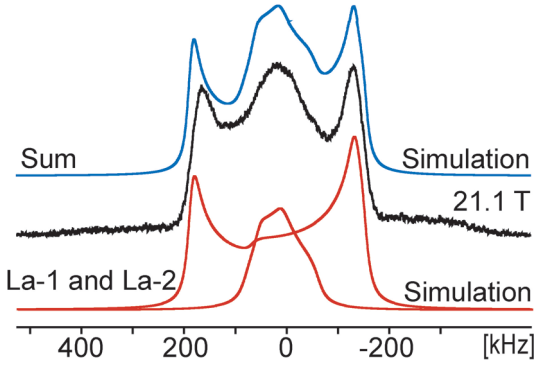

Figure 6. ^{139}La static NMR of $LaLi_{0.5}Fe_{0.2}O_{2.09}$. The spectrum was collected at 21.1 T using a WURST-echo pulse sequence.[18] Simulation was done using the DMFit software.[35] The simulation shows the ^{139}La spectrum consisting of two peaks. The wider peak, La-2, has a C_Q of 56 ± 1 MHz, and η of 0.05 ± 0.05. The peak in the center of the spectrum, La-1, represents a distribution of lanthanum sites. Details are discussed in the main text.

Atomic distributions are known to occur in a variety of compounds, with well-known crystal structures.[34] Studies performed on compounds containing atomic-level distribution usually focus on an element, which is sensitive to the components of its first coordination sphere. Modification of the first coordination sphere of the observed element through different chemical syntheses can change the NMR spectra obtained for the element of interest, and thus the distribution of the elements in the first coordination sphere is mapped through the NMR analysis of different compounds of similar chemical structure.[34] The garnet-like structure $LaLi_{0.5}Fe_{0.2}O_{2.09}$ exhibits a distribution of Li environments that is seen in the ^{7}Li MAS NMR. This system poses a unique challenge because the distribution of Li environments is seen in the ^{7}Li environments themselves, as opposed to a secondary nucleus in the first coordination sphere.

$LaLi_{0.5}Fe_{0.2}O_{2.09}$ was prepared, together with a family of compounds prepared in the same manner, but with variation in the relative amount of Li, Fe, and La. Figure 3b shows the ^{7}Li MAS NMR of $LaLi_{0.5}Fe_{0.2}O_{2.09}$, $La_{0.94}Li_{0.69}Fe_{0.2}O_{2.09}$, and $LaLi_{0.75}Fe_{0.14}O_{2.09}$. It is evident that the ^{7}Li spectrum of each compound includes an array of paramagnetic peaks. Line fit analysis was performed for each of these spectra, and will be discussed further in this paper. It appears that a distribution of paramagnetic peaks exists in each sample, with the ratio of diamagnetic to paramagnetic peaks varying throughout the samples as the stoichiometry is varied.

^{139}La static NMR was used to probe this distribution further. The analysis of $LaLi_{0.5}Fe_{0.2}O_{2.09}$ was performed using a WURST-echo pulse sequence. Two resonances were observed with very different quadrupole parameters, as shown in Figure 6. A WURST-QCPMG pulse sequence was also employed in which a swept pulse of 1 MHz was used.[17] The ^{139}La static solid-state NMR spectra of $LaLi_{0.5}Fe_{0.2}O_{2.09}$, $La_{0.94}Li_{0.69}Fe_{0.2}O_{2.09}$, and $LaLi_{0.75}Fe_{0.14}O_{2.09}$ are shown in Figure 7, panels a, b, and c, respectively.[17]

The optimization of EFG and CSA parameters was sufficient to obtain reasonable fits of the experimental ^{139}La spectra. Line broadening was necessary and different for the two La sites. More line broadening was used in the simulation of La-1, which is closer to the variable Li/Fe/vacant site than La-2. We attribute the necessary line broadening to be primarily the result of the distribution of quadrupole parameters, which results from the distribution of Li, La, and a vacant site. This will be discussed further in this work. There is likely an additional broadening contribution that is a result of a paramagnetic influence of Fe on La line shape in this material, and would also be a larger effect for La-1 than La-2, consistent with the experimental spectra.

When the spectra obtained for $LaLi_{0.5}Fe_{0.2}O_{2.09}$ in Figure 6 and 7 are compared, there is a noticeable difference in the peak in the center of the spectrum. This is due to the sensitivity of the WURST-QCPMG pulse sequence to differences in the T_2 relaxation of the different sites. The center peak (C_Q = 29 MHz ± 2 MHz), with a longer T_2 value than the broader peak (C_Q = 56 MHz ± 1 MHz), is attenuated, with the possibility of some of the features of the quadrupole powder pattern being suppressed. This is not the case when this spectrum is observed with the WURST-echo pulse sequence. Here the intensities of the two peaks are more indicative of the relative stoichiometric amounts of each La site in the sample. The WURST-echo pulse

sequence, Figure 6, is preferred for this sample. However, because of the much longer acquisition time it was not feasible to obtain a WURST-echo measurement for each material.

These spectra, Figure 7, outline two La sites in each material, as shown in the simulations. One of these sites is common to all of these materials, and is responsible for a broad, axial site with a C_Q of 56 ± 1 MHz and asymmetry parameter, η of 0.05 ± 0.05, while the other peak, which is superimposed on the first one, changes throughout the samples and appears to represent a La site that changes, depending on the composition of the sample.[19] On further examination of the crystal structure of the material, it is evident that one of the La sites (La-2) is far from the variable site at (0.25, 0.25, 0.25) which is occupied by Li, iron, or a vacancy (4.485 Å), while the other (La-1) is close to the variable site at (0.25, 0.25, 0.25) (3.2 Å), shown in Figure 8. This means that variation in the La NMR between samples is likely due to this variable site at (0.25, 0.25, 0.25). The differing occupancy of this site creates different La environments through the changing of the electric field gradient of the La atom, which is very sensitive to its environment.[36] The broad axial NMR line shape that represents La-2 is consistent with a single La site that is in a nonspherical oxygen environment, which lies on the axis of a 4-fold rotation and a 4-fold rotoinversion.[19]

The narrower line shape of La-1 is due to the lack of symmetry, specifically, less than 3-fold rotational symmetry. Simulation of the NMR spectra revealed that La-1 has a C_Q of 29 MHz ± 2 MHz and an asymmetry parameter, η of 0.6 ± 0.1.[19] The simulation of this site involved a considerable amount of line broadening, which is an indication that this is not a single site, but a distribution of lanthanum sites with a variation in the values of C_Q and η. Figure 8 illustrates the distance of La from the variable

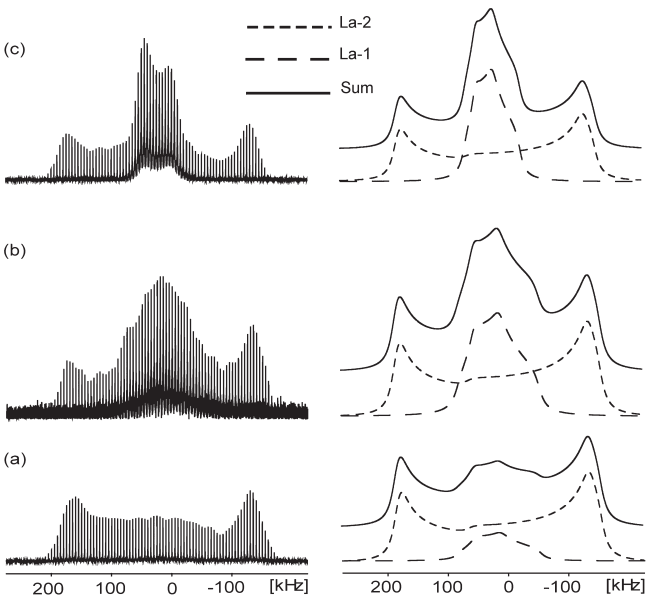

Figure 7. ^{139}La static solid-state NMR of (a) $LaLi_{0.5}Fe_{0.2}O_{2.09}$, (b) $La_{0.94}Li_{0.69}Fe_{0.2}O_{2.09}$, and (c) $LaLi_{0.75}Fe_{0.14}O_{2.09}$. Spectra were acquired at 21.1 T using the WURST-QCPMG pulse sequence.[17] Simulations were performed using DMFit software.[35]

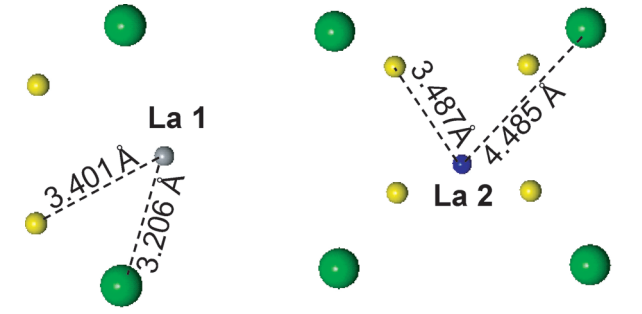

Figure 8. La-1 and La-2 crystallographic environments. Green spheres represent Fe-2, which may be replaced by Li or a vacancy; yellow spheres represent Li; the gray sphere represents La-1 (Left); and the blue sphere represents La-2 (Right). Left: La-1, with a distance of 3.206 Å to Fe-2. Right: La-2. Images were created in XtalDraw.[33] Distances between La and Fe/Li have been included in each case within 5 Å.

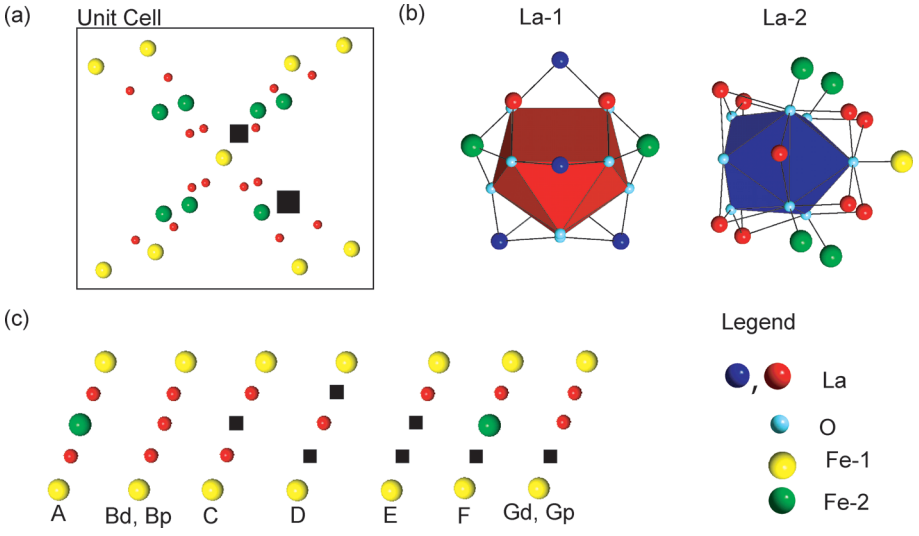

Figure 9. (a) $LaLi_{0.5}Fe_{0.2}O_{2.09}$ unit cell showing possible positions of vacancies. The positions of La-1 and La-2 are not shown here for clarity. Black squares represent potential vacancies in the cell. (b) Polyhedra representing the La-1 and La-2 local environments in the crystal structure. (c) A through G represent the potential distributions of Li, iron, and a vacant site showing half of the body diagonal of the unit cell in the Left of this figure. The legend presented can be applied to (a), (b), and (c). The full unit cell of this material is shown in Figure 5, including the placement of the La atoms in the unit cell.

dx.doi.org/10.1021/cm200823p |*Chem. Mater.* 2011, 23, 3105–3113

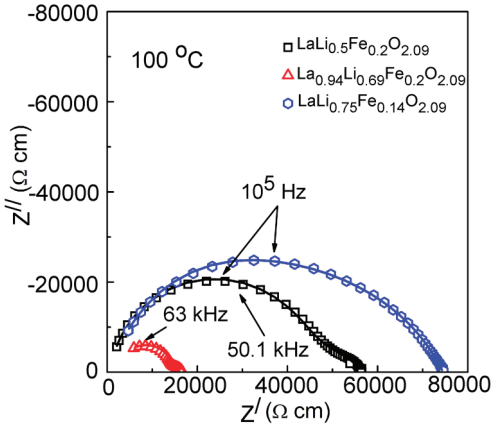

Figure 10. Typical AC impedance plots at 100 °C for Fe based garnet-like structure.

Table 3. Fitting Parameters of Impedance Plots at 100 °C of $LaLi_{0.5}Fe_{0.2}O_{2.09}$, $La_{0.94}Li_{0.69}Fe_{0.2}O_{2.09}$, and $LaLi_{0.75}Fe_{0.14}O_{2.09}$ at 850 °C Sintering Temperature

compound[a]	$R_{(H-F)}$ (Ω)	$Q_{(H-F)}$ (pF)	η	$R_{(L-F)}$ (Ω)	$Q_{(L-F)}$ (nF)	η
$LaLi_{0.5}Fe_{0.2}O_{2.09}$	212030	6.4	0.94	64528	29.6	0.61
$La_{0.94}Li_{0.69}Fe_{0.2}O_{2.09}$	4982	0.00254	0.68	18721	13.4	1.0
$LaLi_{0.75}Fe_{0.14}O_{2.09}$	29680	11.1	1.0	122640	0.77	0.71

[a] χ^2 values of all fitted plots are less than 10^{-3} to ensure high confidence in results.

site, Fe-2, in this material. It is clear that La-2 is far from this source, while La-1 is close. This is the reason for the differences in the necessary line broadening for these two La sites, and this supports the hypothesis that Li is distributed throughout this material, showing a range of Li environments, which affects those of La. From the series of ^{139}La spectra of the related materials, shown in Figure 6, it is shown that as the composition of these materials change, the distribution of the La-1 environments is affected. This is consistent with the changing distribution seen for the lithium environments, shown in Figure 3.

This complex family of materials can be further examined by considering the different possible lithium environments present. Using the measured ^{139}La and ^{7}Li NMR spectra, along with crystallographic data, the Li sites found in the ^{7}Li spectra can be tentatively assigned with the following assumptions:

(1) Li peaks will be more resolved and have a higher chemical shift if the respective Li site is close to iron.
(2) Li peaks will have a chemical shift close to 0 ppm, if the respective Li is far from iron.

Some configurations contribute more than one peak in the ^{7}Li NMR spectrum. By comparison, in configuration A (Figure 9), with no Li substituting Fe-2, the two Li atoms are chemically and magnetically equivalent; however, in configuration B there are two "types" of Li present: the Li atoms close to the Fe-1 site (yellow spheres) will have a more paramagnetic nature because of their proximity to the iron, whereas the Li in the center of the configuration is farther from iron, and will have a more diamagnetic nature. Thus, configuration B will contribute two peaks to the ^{7}Li NMR spectrum. With this consideration, the combination of all of these configurations in any compound will contribute nine peaks in the ^{7}Li NMR spectrum. This is consistent with what is seen in the ^{7}Li MAS NMR, shown in Figure 3, which shows multiple lithium sites.

When we consider the ^{7}Li MAS NMR of these materials, it is not immediately obvious that the distribution of the Li, iron, and vacancy is changing throughout the materials. However, when the ^{7}Li MAS NMR is combined with the ^{139}La NMR the change in the materials becomes evident as their composition changes. As the Li/Fe ratio increases in the samples, the diamagnetic peak in the ^{7}Li MAS NMR increases; this is possibly due to the filling of vacant sites in the (0.25, 0.25, 0.25) position. This site-filling has a dramatic effect on the EFG of La-1, and this is seen as a change in the ^{139}La NMR, where the central peak changes in appearance.

It should be noted here that the ^{7}Li MAS NMR peak assignment is a complicated endeavor, and it is possible that there are more permutations of the atomic distribution than indicated here. The aim here is not to specifically assign the peaks in the NMR spectra, but to illustrate the complexity of this material, and understand how this atomic distribution relates to the ionic and electronic conductivity of the materials.

AC Electrical Conductivity. Electrochemical alternating current (AC) impedance spectroscopy in the frequency range of 0.01 Hz−1 MHz was used to estimate the electrical conductivity of Fe-based garnet related structure compounds. Shown in Figure 10 are the typical impedance plots of $LaLi_{0.5}Fe_{0.2}O_{2.09}$, $La_{0.94}Li_{0.69}Fe_{0.2}O_{2.09}$, and $LaLi_{0.75}Fe_{0.14}O_{2.09}$. The impedance plots can be modeled using an equivalent circuit consisting of resistance (R) and constant phase element (Q). Table 3 lists the typical fitting parameters of AC impedance data. The capacitance value for the high-frequency (H-F) and low-frequency (L-F) semicircle was calculated using the expression:[37,38]

$$C = R^{\left(\frac{1-\eta}{\eta}\right)} Q^{\left(\frac{1}{\eta}\right)}$$

where η is the empirical constant which can take any arbitrary value between zero and one.

The capacitance was found to be in the range of pF and μF, suggesting that two semicircles obtained at 100 °C may

dx.doi.org/10.1021/cm200823p |*Chem. Mater.* 2011, 23, 3105–3113

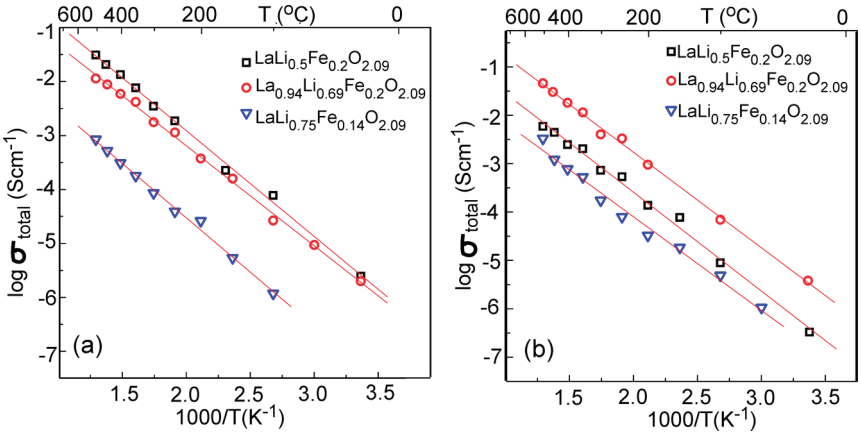

Figure 11. Electrical conductivity of the samples prepared (a) at 800 and (b) 850 °C in air. The line passing through the data point is the best fit and was used to determine the activation energy.

correspond to bulk and electrode contribution to the total conductivity. Unlike well-known garnet-like materials, $Li_5La_3M_2O_{12}$ and $Li_6ALa_2M_2O_{12}$ (A = Ca, Sr, Ba; M = Nb, Ta), the investigated Fe compounds clearly show absence of tail at the L-F side, indicating that electrode−electrolyte interface is reversible. In the present case, Au is blocking for Li ions and reversible for electrons; thus, it clearly indicates significant electronic conduction in Fe garnets. This is consistent with the large amount of Fe in the structure. The shape of the impedance plots is highly reversible during the heating and cooling cycles.

Unlike other garnets, the La−Li−Fe samples were found to have poor mechanical stability. Hence, it was difficult to perform electron blocking electrode direct current (DC) measurements to separate ionic conductivity. The low-frequency intercept has been used to determine the electrical conductivity. Figure 11 shows the Arrhenius plots for electrical conductivity of the investigated La−Li−Fe-garnets. Ramzy and Thangadurai showed recently that there is a direct correlation between the concentration of lithium and the electrical conductivity for compounds involving substitution of Li in place of other cations.[9] However, in this case, the conductivity is seen to decrease relative to the parent materials.

The decrease in conductivity, relative to the parent composition, may be due to poor density of the samples. Unfortunately, these Li−La−Fe samples densities cannot be determined because of their chemical reaction with water, and hence, we were unable to discuss them in conjunction with their density. At a sintering temperature of 800 °C, the parent compound $LaLi_{0.5}Fe_{0.2}O_{2.09}$, offers the highest conductivity of $\sim 10^{-5}$ S cm^{-1} at room temperature (23 °C) and reaches $\sim 10^{-1.5}$ S cm^{-1} at 500 °C. The activation energy for electrical conductivity was found to be 0.43, 0.39, and 0.41 eV for $LaLi_{0.5}Fe_{0.2}O_{2.09}$, $La_{0.94}Li_{0.69}Fe_{0.2}O_{2.09}$, and $LaLi_{0.75}Fe_{0.14}O_{2.09}$, respectively, for the samples prepared at 850 °C. The activation energy for electrical conduction was found to be within the range reported for the garnet-type solid electrolytes and other solid Li ion electrolytes.[34]

It is observed here that the conductivity of these materials is not increased with increasing lithium content, and moreover, that the conductivity decreases with the increase in the intensity of the diamagnetic peak, relative to the paramagnetic peaks, in both the ^{7}Li and ^{139}La NMR data sets. This would suggest that conductivity is impeded by the presence of lithium on the Fe-2 sites of the material. These lithium resonances, observed in the diamagnetic region of the spectrum, arise as a result of substitution of lithium into the Fe site; thus, it appears that additional lithium in the structure is present in sites which do not favor electrical conductivity. In future work this family of materials will be studied to probe the nature of Li ion dynamics through systematic electrochemical cycling and NMR.

CONCLUSIONS

The $LaLi_{0.5}Fe_{0.2}O_{2.09}$ family of compounds has been studied using ^{7}Li MAS and ^{139}La static solid-state NMR, as well as bulk electronic conductivity measurements. It has been shown that the combination of these two very different NMR techniques is useful for the structural evaluation of complex materials. ^{7}Li MAS NMR is very sensitive to Li environments, and can be used to distinguish between very different Li environments, and the combination of ^{7}Li MAS NMR and ^{139}La NMR is a powerful tool for evaluating such complex structures. Knowing the structure of these compounds is the first step to uncovering the mechanism of Li ion dynamics in these materials and understanding the process of Li migration through vacancy-mediated conductivity. The electrical conductivity of the samples was found to depend on Li content. The parent compound $LaLi_{0.5}Fe_{0.2}O_{2.09}$ offers the highest conductivity of $\sim 10^{-5}$ S cm^{-1} at room temperature (23 °C), and reaches a conductivity of $\sim 10^{-1.5}$ S cm^{-1} at 500 °C.

AUTHOR INFORMATION

Corresponding Author

*E-mail: goward@mcmaster.ca (G.R.G.), vthangad@ucalgary.ca (V.T.). Phone: (905)-525-9140, x24176 (G.R.G.), (403)-210-8649 (V.T.). Fax: (905)-522-2509 (G.R.G.), (403)-289-9488 (V.T.).

ACKNOWLEDGMENT

This research is supported by the AUTO21 Network of Centres of Excellence, Canada's national automotive research and development program. For access to the 900 MHz NMR spectrometer, the authors would also like to thank the National Ultrahigh-Field NMR facility for Solids (Ottawa, Canada), a national research facility funded by the Canadian Foundation for Innovation, the Ontario Innovation Trust, Recherche Québec,

the National Research Council Canada, and Bruker BioSpin and managed by the University of Ottawa. The authors are grateful for assistance and helpful discussions provided by Dr. Victor Terskikh and Dr. Eric Ye, as well as helpful discussions with Prof. A.D. Bain.

REFERENCES

(1) Thangadurai, V.; Adams, S.; Weppner, W. *Chem. Mater.* **2004**, *16*, 2998–3006.
(2) Cussen, E. J. *Chem. Commun.* **2006**, 412–413.
(3) van Wüllen, L.; Echelmeyer, T.; Meyer, H. W.; Wilmer, D. *Phys. Chem. Chem. Phys.* **2007**, *9*, 3298–3303.
(4) Antonini, B.; Geller, S.; Paoletti, A.; Paroli, P.; Tucciarone, A. *Phys. Rev. Lett.* **1978**, *41*, 1556–1558.
(5) Ilmer, M.; Grabmaier, B. C.; Blasse, G. *Chem. Mater.* **1994**, *6*, 204–206.
(6) Wilkening, M.; Heine, J.; Lyness, C.; Armstrong, A. R.; Bruce, P. G. *Physical Review B* **2009**, *80*, 064302.
(7) O'Callaghan, M. P.; Powell, A. S.; Titman, J. J.; Chen, G. Z.; Cussen, E. J. *Chem. Mater.* **2008**, *20*, 2360–2369.
(8) Kuhn, A.; Narayanan, S.; Spencer, L.; Goward, G.; Thangadurai, V.; Wilkening, M. *Phys. Rev. B* **2011**, *83*, 094302-1−094302-11.
(9) Ramzy, A.; Thangadurai, V. *ACS Appl. Mater. Interfaces* **2010**, *2*, 385–390.
(10) O'Callaghan, M. P.; Cussen, E. J. *Chem. Commun.* **2007**, 2048–2050.
(11) Koch, B.; Vogel, M. *Solid State Nucl. Magn. Reson.* **2008**, *34*, 37–43.
(12) O'Callaghan, M. P.; Cussen, E. J. *Solid State Sci.* **2008**, *10*, 390–395.
(13) Xu, Z.; Stebbins, J. F. *Solid State Nucl. Magn. Reson.* **1995**, *5*, 103–112.
(14) Cahill, L. S.; Chapman, R. P.; Kirby, C. W.; Goward, G. R. *Appl. Magn. Reson.* **2007**, *32*, 565–581.
(15) Lee, Y. J.; Wang, F.; Grey, C. P. *J. Am. Chem. Soc.* **1998**, *120*, 12601–12613.
(16) Ooms, K. J.; Feindel, K. W.; Willans, M. J.; Wasylishen, R. E.; Hanna, J. V.; Pike, K. J.; Smith, M. E. *Solid State Nucl. Magn. Reson.* **2005**, *28*, 125–134.
(17) O'Dell, L. A.; Schurko, R. W. *Chem. Phys. Lett.* **2008**, *464*, 97–102.
(18) Bhattacharyya, R.; Frydman, L. *J. Chem. Phys.* **2007**, *127*, 194503-1–194503-8.
(19) Spencer, L.; Coomes, E.; Ye, E.; Terskikh, V.; Ramzy, A.; Thangadurai, V.; Goward, G. R. *Can. J. Chem.* **2011**.
(20) Bastow, T. J.; Mathews, T.; Sellar, J. R. *Solid State Ionics* **2004**, *175*, 129–133.
(21) Massiot, D.; Farnan, I.; Gautier, N.; Trumeau, D.; Trokiner, A.; Coutures, J. P. *Solid State Nucl. Magn. Reson.* **1995**, *4*, 241–248.
(22) Medek, A.; Frydman, V.; Frydman, L. *J. Phys. Chem. A* **1999**, *103*, 4830–4835.
(23) Abbattista, F.; Mazza, D.; Vallino, M.; Gazzano, M. *J. Less-Common Met.* **1988**, *144*, 311–319.
(24) Mazza, D.; Abbatista, F.; Vallino, M.; Ivaldi, G. *J. Less-Common Met.* **1985**, *106*, 277–285.
(25) Hyooma, H.; Hayashi, K. *Mater. Res. Bull.* **1988**, *23*, 1399–1407.
(26) Ohzuku, T.; Ariyoshi, K.; Takeda, S.; Sakai, Y. *Electrochim. Acta* **2001**, *46*, 2327–2336.
(27) Thangadurai, V.; Schwenzel, J.; Weppner, W. *Ionics* **2005**, *11*, 11–23.
(28) Chen, J.; Wang, S.; Whittingham, M. S. *J. Power Sources* **2007**, *174*, 442–448.
(29) Larson, A. C.; Dreele, R. B. V. *Los Alamos National Laboratory Report LAUR 86-748*; Los Alamos National Laboratory: Los Alamos, NM, 1994.
(30) Masaki, N.; Doi, K.; Nasu, S.; Tanifuji, T.; Uchida, K. *J. Nucl. Mater.* **1979**, *84*, 341–342.
(31) Duer, M. J. *Introduction to Solid-State NMR Spectroscopy*; Blackwell Science, Oxford, U.K., 2004.
(32) Grey, C. P.; Lee, Y. J. *Solid State Sci.* **2003**, *5*, 883–894.
(33) Downs, R. T.; Sinnaswamy, K. *XtalDraw*; University of Arizona: Tucson, AZ, 2003.
(34) Ashbrook, S. E.; Whittle, K. R.; Lumpkin, G. R.; Farnan, I. *J. Phys. Chem. B* **2006**, *110*, 10358–10364.
(35) Massiot, D.; Fayon, F.; Capron, M.; King, I.; Le Calve, S.; Alonso, B.; Durand, J. O.; Bujoli, B.; Gan, Z. H.; Hoatson, G. *Magn. Reson. Chem.* **2002**, *40*, 70–76.
(36) Hamaed, H.; Lo, A. Y. H.; Lee, D. S.; Evans, W. J.; Schurko, R. W. *J. Am. Chem. Soc.* **2006**, *128*, 12638–12639.
(37) Chinarro, E.; Jurado, J. R.; Figueiredo, F. M.; Frade, J. R. *Solid State Ionics* **2003**, *160*, 161–168.
(38) Li, Q.; Thangadurai, V. *Fuel Cells* **2009**, *9*, 684–698.